

# Meter-class Mirror Figure Metrology Using a 24-Channel Fiber Interferometer

Ronald Holzlöhner<sup>a</sup>, Samuel Lévêque<sup>a</sup>, Nicola Di Lieto<sup>a</sup>, Juan-Antonio Marrero Hernández<sup>a</sup>,  
Andrew P. Rakich<sup>b,a</sup>

<sup>a</sup> European Southern Observatory, Karl-Schwarzschild Straße 2, D-85748 Garching, Germany

<sup>b</sup> Giant Magellan Telescope Organization, Pasadena, CA, US2

## ABSTRACT

We measured the influence functions of a 9-actuator warping harness of an ELT primary mirror segment prototype using a fiber interferometer. The compact setup consists of a stiff, lightweighted aluminium plate with a similar diameter as the segment (1.25 m), holding 24 fiber-fed collimators arranged in three concentric rings. We measure simultaneously the 24 absolute distances to the mirror surface with a nominal precision of 0.5 ppm. The recorded noise level in a quiet environment was below 50 nm rms. We found good agreement between the measured influence functions and the finite-element model by the segment support manufacturer. These measurements were performed at ESO Garching in June 2017, with the “Absolute Multiline” metrology system.

**Keywords:** Wavefront Control, Segmented Mirrors, Warping Harness. Phasing

## 1. INTRODUCTION

This paper describes the measurements of the shape variation of an ELT segment prototype from the FEED B campaign made by SAGEM and CESA [1], generated by its segment support warping harness. The measurements were performed at ESO Garching in June 2017 with the “Absolute Multiline” metrology system from Etalon AG [2].

### Rationale and objectives

The need for the direct measurement of the optical surface deformation of an E-ELT M1 segment sub-unit has been previously, under the following load cases:

1. *Actuation of the warping harnesses*, for enabling the direct measurement of the warping harness influence functions, without relying on a large interferometric test set-up.
2. *Gravity load under various telescope elevation angles*, for enabling the direct verification of finite-element model predictions, for which no interferometric set-up can be practically implemented.

Based on ESO’s experience with the “Absolute Multiline” system, it was recognized that this system may actually allow segment deformation measurements on its own, although at a reduced but still acceptable spatial resolution. This finding triggered a proposal for building a segment figure metrology system using a stiff plate holding 24 absolute distance measurement interferometers of the “Absolute Multiline” above an ELT mirror segment prototype.

The main design characteristics are summarized below:

1. 24 fiber collimators are mounted onto a stiff lightweighted circular aluminium plate. Each collimator accepts an optical single-mode fiber connected to the Multiline system.
2. The plate is then mounted approximately 110 mm above a mirror segment and each collimator is aligned to the local mirror surface normal.
3. The Multiline system generates a fiber interferometer between the mirror and the fiber tips and measures all 24 distances ( $D_1, \dots, D_{24}$ ) in parallel, with a precision of 0.5  $\mu\text{m/m}$ .
4. The collimators are arranged in patterns of three concentric rings in which they are equally spaced.

5. Tip/tilt and lateral displacement errors of the plate vs. the mirror generate small amounts of spurious coma and astigmatism that can be calibrated out (e.g. 13 nm RMS astigmatism per mrad plate tip/tilt).

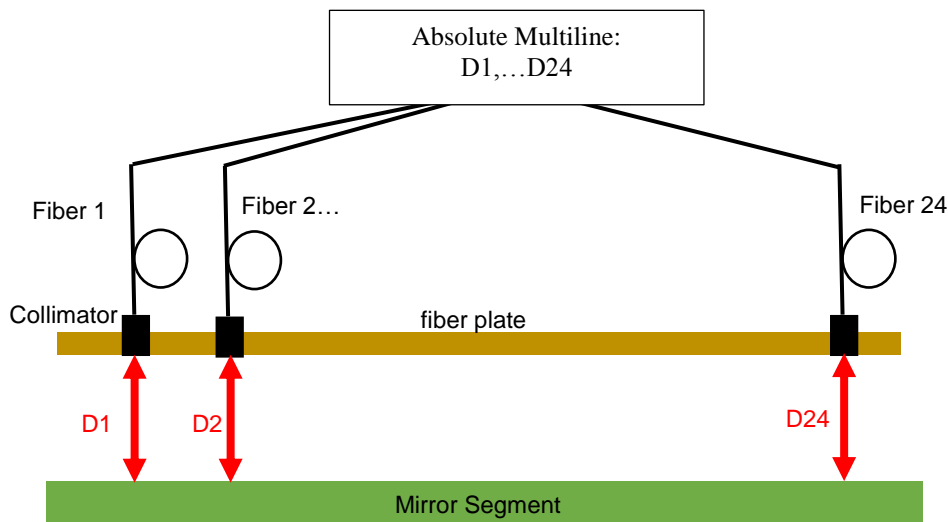


Figure 1. Measurement principle of the mirror segment shape using the “Absolute Multiline”. The mean distance between the fiber plate and the mirror segment is about 110 mm.

## 2. DESIGN

### Description of the “Absolute Multiline”

The current version of the “Absolute Multiline” allows absolute length measurements with a precision of 0.5  $\mu\text{m}/\text{m}$  over 20 m, on up to 24 channels simultaneously. It is based on laser frequency scanning interferometry, calibrated by atomic transitions provided by an on-board gas cell.

The deformation of large structures can be monitored by a set of appropriately configured measurement beams with a data rate of typically several Hertz. In addition, vibrations of an object  $\gg 1$  kHz can be measured during a typically 1s time window (burst mode). The measurement path is defined between the tip of an optical fiber and a reflective surface. The length of the optical fiber can be several hundred meters and the fiber can easily be routed through cable wraps towards areas with limited access. The laser beam can be interrupted at any time without causing precision loss. The absolute distance is recovered at the next sampling period.

The Multiline has been already tested in Garching and on the VLT/UT4 to demonstrate its ability to accurately monitor the rigid body motion of telescope mirrors in representative operation conditions.

Tests conducted by CERN<sup>1</sup> have shown that the differential error between all channels of the multiline is limited to about 10 nm rms.

---

<sup>1</sup> Private communication

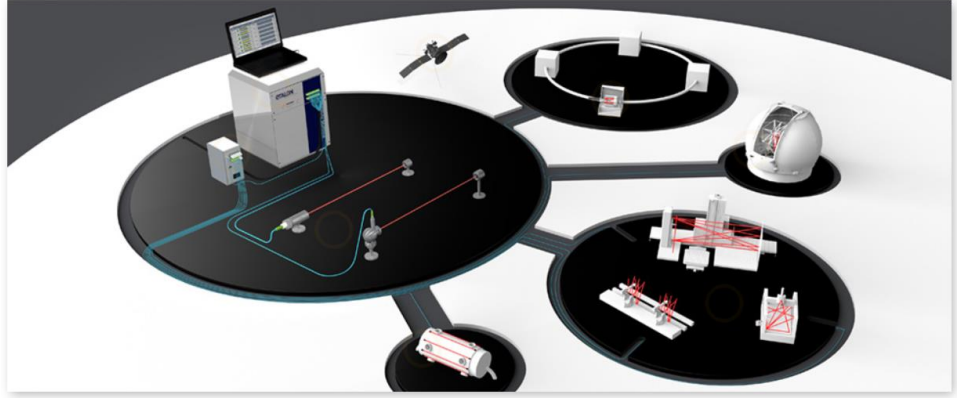


Figure 2. Left: Multiline hardware (excluding the fibers); Right: example of fields of application of the Multiline, as reported in [www.etalon.com](http://www.etalon.com), showing the versatility of this metrology system

### Definition of the optimum location of the sensors

A dedicated study has been conducted to optimize the 24 collimator positions and determine which optical aberrations can be measured based on the Singular Value Decomposition (SVD), finding that the first 15 Zernike modes (up to and including tetrafoil) can be concurrently measured at high accuracy.

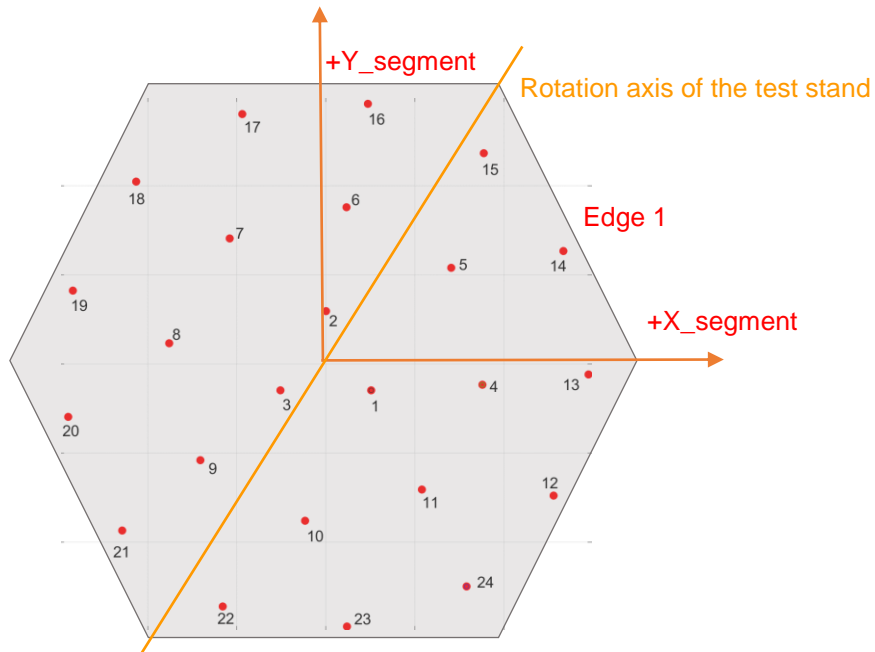


Figure 3. Fiber position (top view)

The 24 fiber collimators of type PAF-X-18-PC-C were purchased from Thorlabs. The beam collimation is provided by an aspheric lens ( $f = 18.4 \text{ mm}$ ) operating in the measurement wavelength range 1050 – 1620 nm. The output beam waist diameter is 3.49 mm. The field of view of the 9 micron core fiber is  $\pm 0.24 \text{ mrad}$  or about  $\pm 0.8 \text{ arcmin}$ . This angle corresponds to the maximal slope between the fiber collimator and the local surface of the mirror segment before losing the laser beam retro-injected in the single-mode fiber.

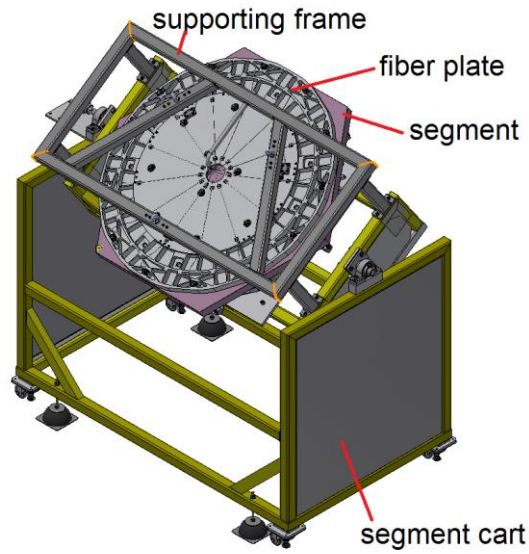


Figure 4. Test setup on segment cart



Figure 5. Fiber collimators used in the experiment

## Design of the fiber plate and supporting frames

The circular fiber plate is made of a lightweighted aluminium alloy (diameter 1.24 m). It is supported above the segment at 3 points in a closely isostatic manner to minimize transmission of warping loads from the support structure. Three pairs of thin rods provide the interface to the supporting steel frame.

The segment is attached to the already existing “M1 segment handling cart”, to which counterweights needed to be added for mass balancing of the extra equipment placed on top, allowing a smooth rotation of the segment in elevation. The cart has also been equipped with rubber feet to reduce the transmission of vibrations.

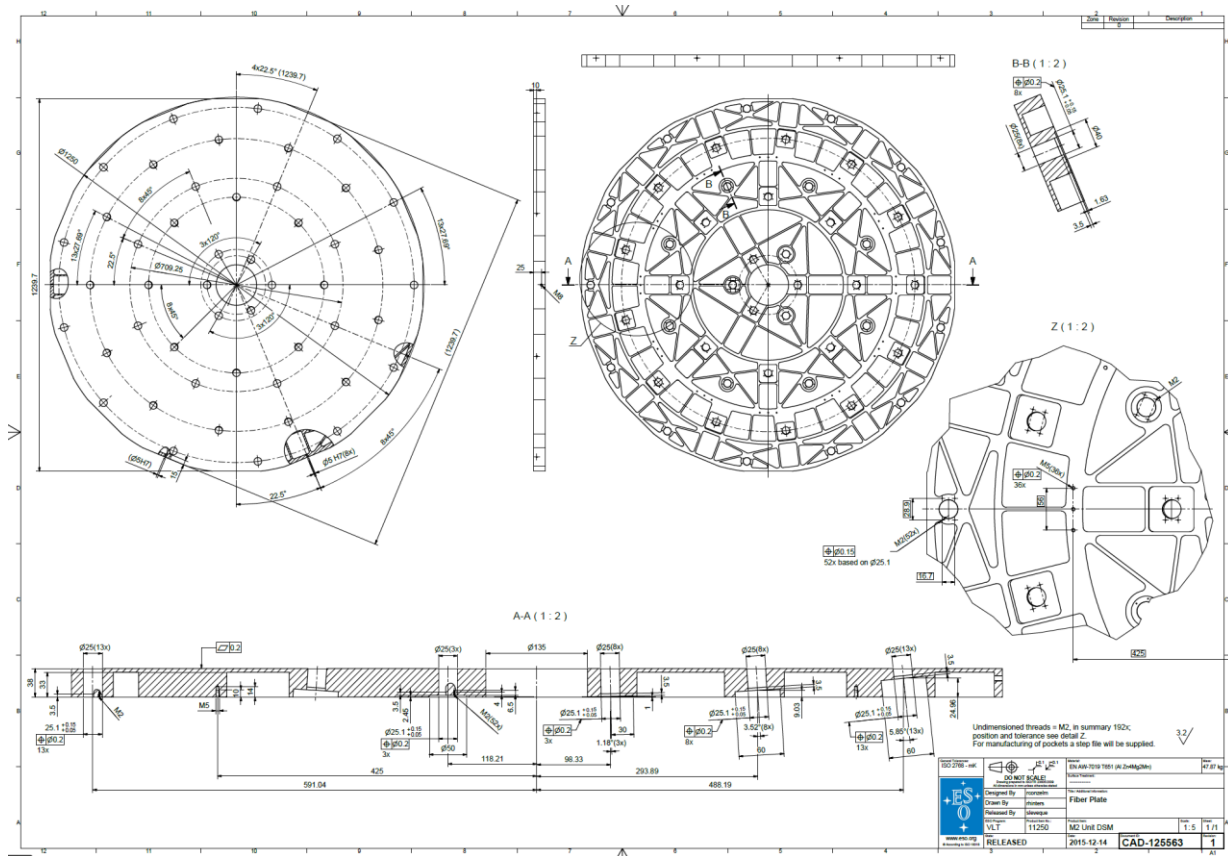


Figure 6. Fiber plate

The fiber plate and the supporting frame were designed to minimize the plate non-rigid body deformation (i.e. except piston and tip/tilt movement) due to the change of the elevation angle of the segment. The expected deformation for a 90° angle of elevation change is 1.8 μm rms surface error over the 24 sensor positions. The computed sensitivity to temperature change is 127 nm/degree rms surface error over the 24 sensor positions.

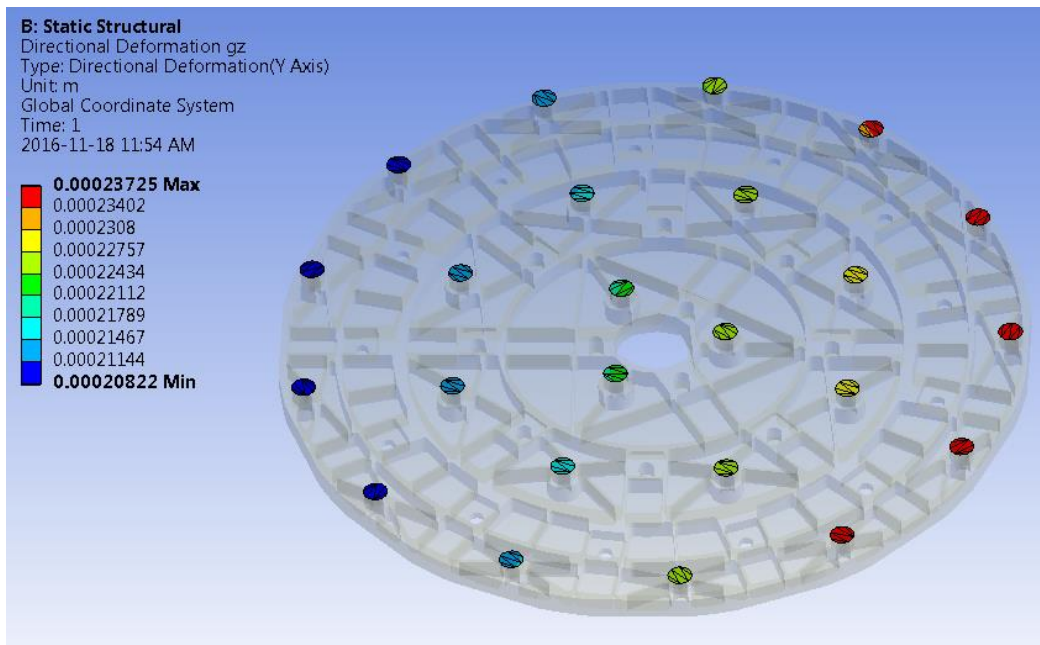


Figure 7. Fiber plate FEM results

### Control hardware and software

The control hardware and software configuration is shown in Figure 8, and further detailed in the following sections. A set of MATLAB scripts have been developed to control the torque generated by each warping harness actuator and to simultaneously read the 24 channels of the Multiline.

These building blocks were then used to automatically record and pre-process data using higher-level MATLAB functions.

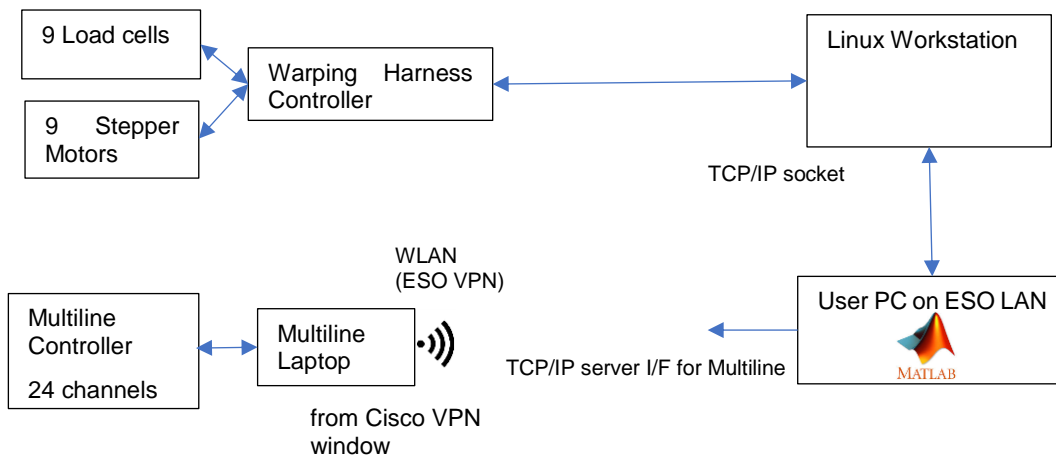


Figure 8. Control configuration

### 3. WARPING HARNESS CONTROL

The stepper motors and strain gauges were controlled using the 1<sup>st</sup> prototype warping harness controller designed at ESO and selected as the solution for the ELT segments.

This activity has resulted in a useful synergy: On one hand, it enabled a reliable operation of the stepper motors, including the ability to remotely control the target strain from a workstation (as illustrated in Figure 8). On the other hand, this enabled the validation of the warping harness controller hardware for the ELT which demonstrated a high reliability through the whole test period.



Figure 9. Warping harness controller (ELT prototype)

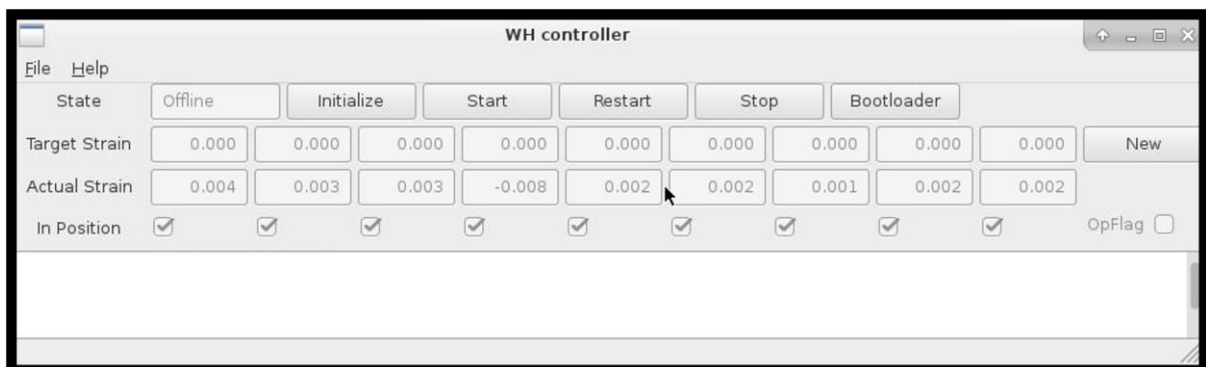


Figure 10. Warping GUI, running on the Linux Workstation

#### Test setup

The test setup is shown in Figure 11, Figure 12 and Figure 13. The hexagonal mirror segment was S3:16.16 SPN03b made of *Astrosital* and polished by SAGEM. It has a thickness of 50 mm and a curvature radius of 76 m, appropriate for a position on the rim of the original 42-meter primary mirror design of the ELT. The segment support is designated CESA-ESO1. Among the total 12 motors, only 9 were connected for compatibility with the ELT warping harness controller prototype. The external motors 1,5 and 9 (HW labels) were not connected (hence one per 120° sector; see Figure 13). We observed that all external motors do have a risk of collision with their tripods (as reported in Figure 13) and had to calibrate the commands limits accordingly.

Although we checked prior to the rental period that the Multiline could be operated on an uncoated mirror surface, the limited alignment sensitivity of the fiber collimators finally prevented us to align all 24 fiber collimators in a reasonable time (i.e. compatible with the limited rental period). These collimators had been chosen as a compromise between stability and cost of about 500 Euro apiece.

Using one aligned collimator, we demonstrated that we could operate the Multiline while tilting the whole mirror assembly to generate different gravity loads. We could also easily align some collimators using small flat coated mirrors located on the segment surface, confirming that we were essentially limited by the fact that the mirror segment was uncoated. In order to complete our test within the rental period, we finally positioned 24 half-inch retroreflectors on the mirror surface, which allowed to immediately detect all metrology signals. This configuration was used to test our ability to measure the warping harness influence function, but it did not allow us to test the gravity load case since the retroreflectors would have fallen off the segment.

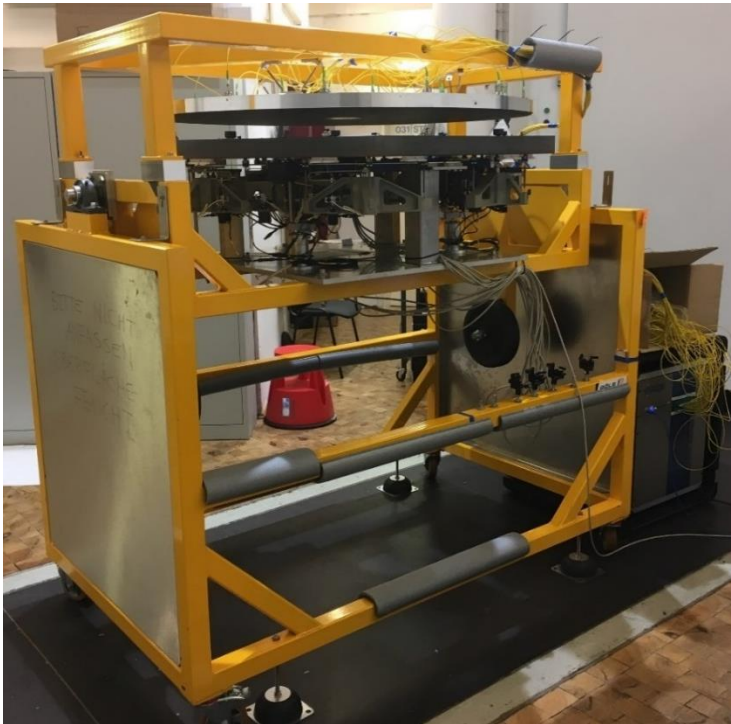


Figure 11. Finished test setup

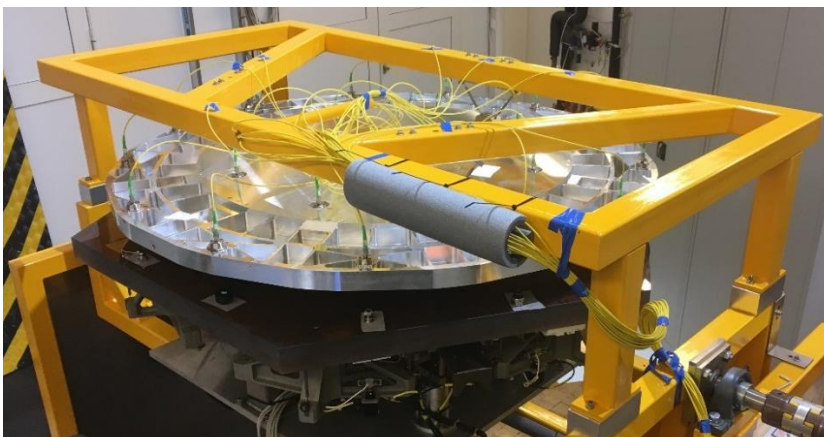


Figure 12. Closer look at the fiber plate

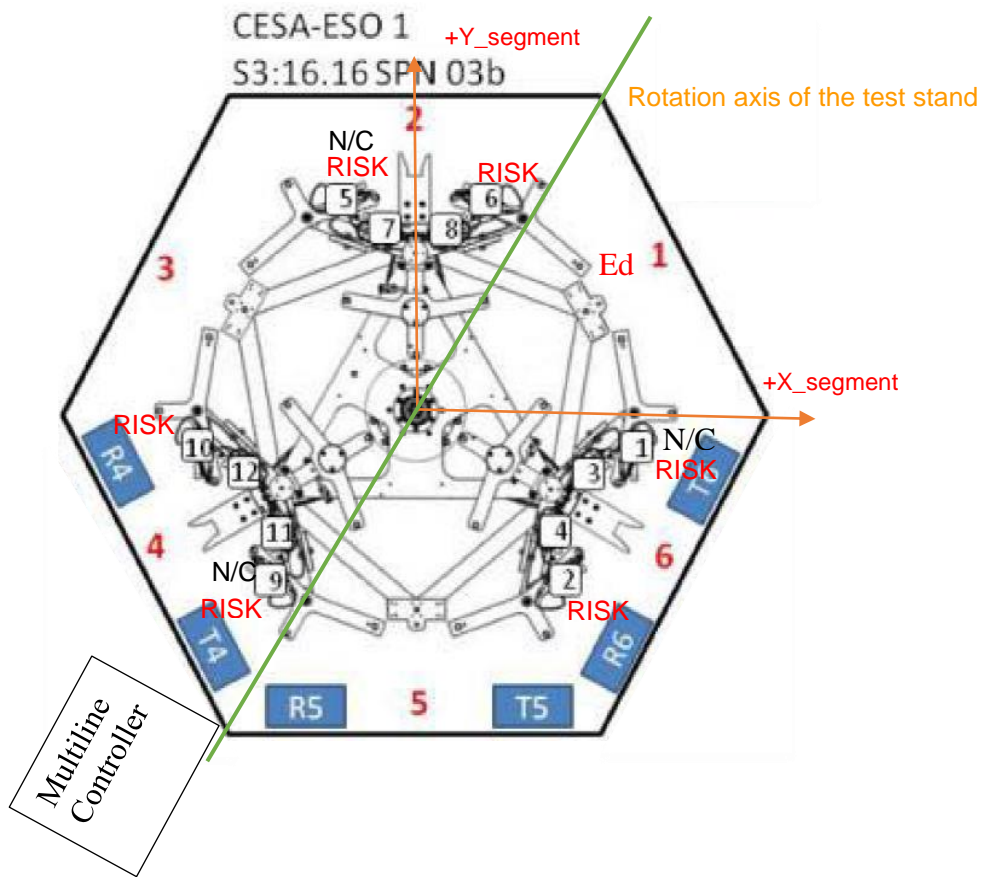


Figure 13. HW configuration, top view (through glass)

#### 4. TEST RESULTS

Overnight measurements have been recorded from 17h30 to 11h15 the day after with all motors set to zero, i.e. without any actuation. The 24 distances were simultaneously logged every 40 s. Figure 14 shows the statistics (std or PTV) of the difference between 2 consecutive sets of 24 measurements.

The noise level appears to be below 50 nm rms (i.e. all modes) before 8h00 (index 1200). A higher noise is observed after index 1200 (8h00 the day after) and attributed to the start of lab activities.

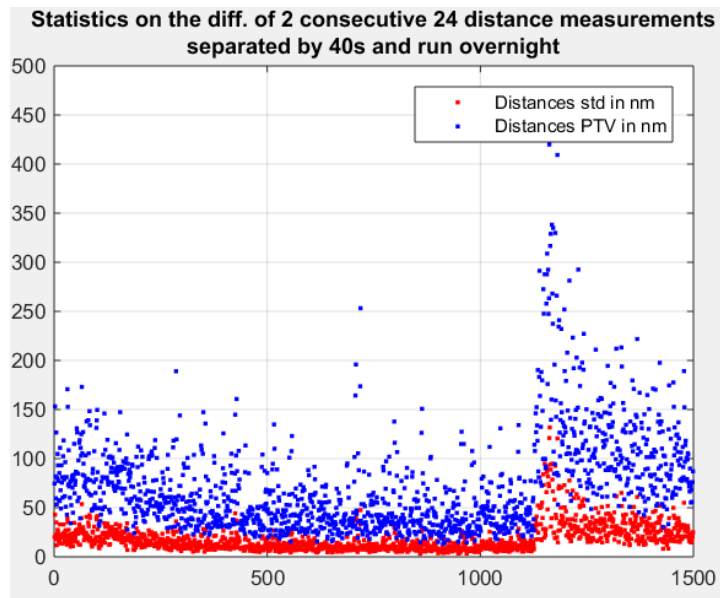


Figure 14. Indication of the measurement noise (all distances)

The evolution of the segment shape between two measurements separated by 40s is calculated by fitting the first 11 Zernike modes to the 24 measurements. The variation of the segment shape is dominated by Piston, Tip, Tilt (i.e. rigid body motion), followed by focus. Focus has a contribution below 10 nm rms over the first 1000 data points as shown in Figure 16. Otherwise, we observe a very small amount of coma (potentially due to a lateral displacement of the fiber plate) and spherical which may be due to a leakage of Piston to spherical. These assumptions remain to be validated.

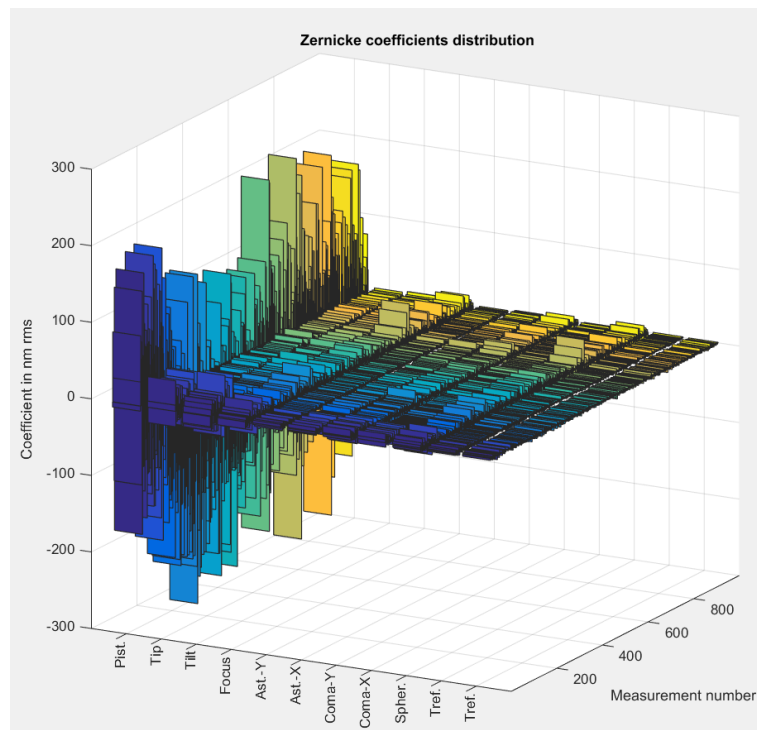


Figure 15. Zernike decomposition of the segment shape difference between 2 consecutive measurements separated by 40 s (overnight). Data obtained after 8h00 are excluded.

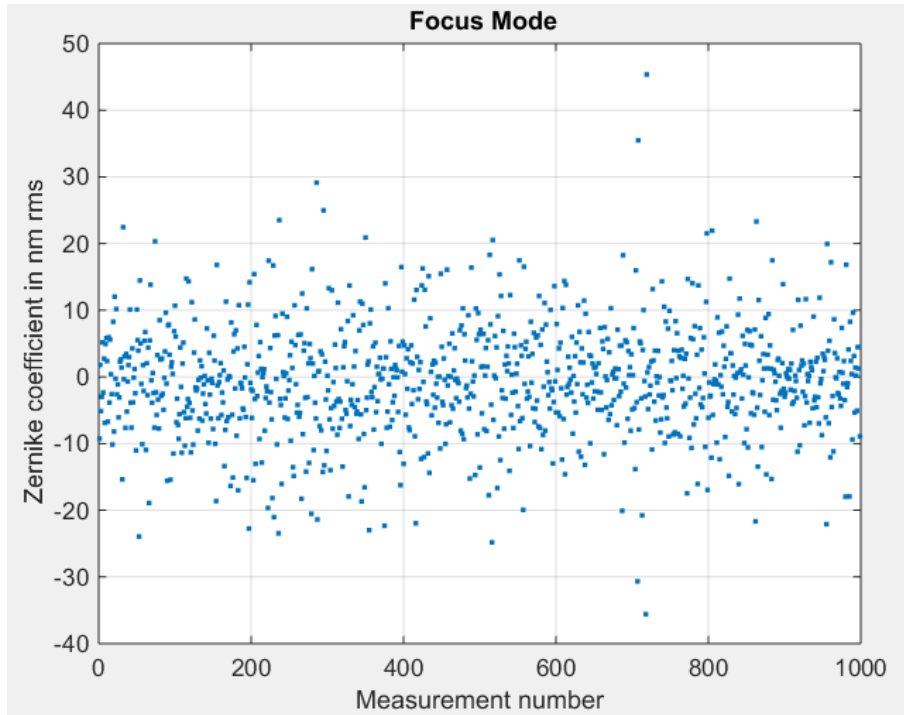


Figure 16. Detail of the Zernike coefficient of the focus mode

**Test of Observability/Commandability of the focus mode**

This test was performed by actuating all internal warping harness motors alternatively from 0 to -1 (mV/V), 25 times. This “Woofers” mode is clearly detected as shown in Figure 17. Focus modeIt introduces about 600 nm rms of focus.

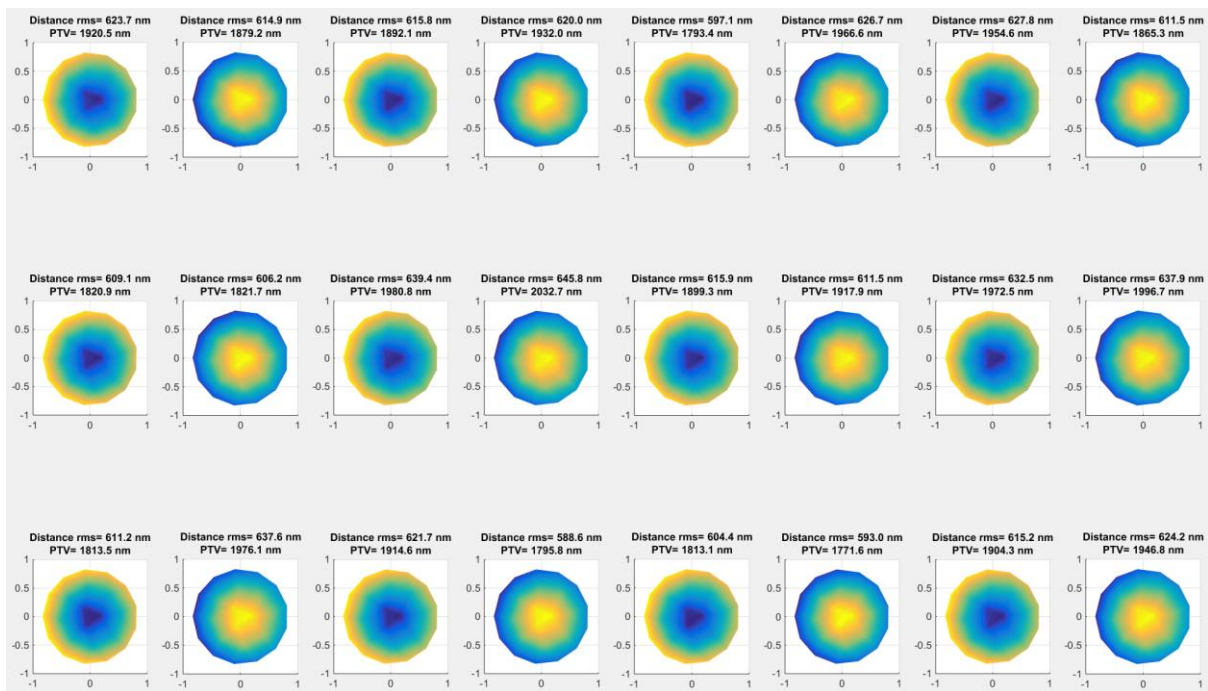


Figure 17. Focus mode shapes

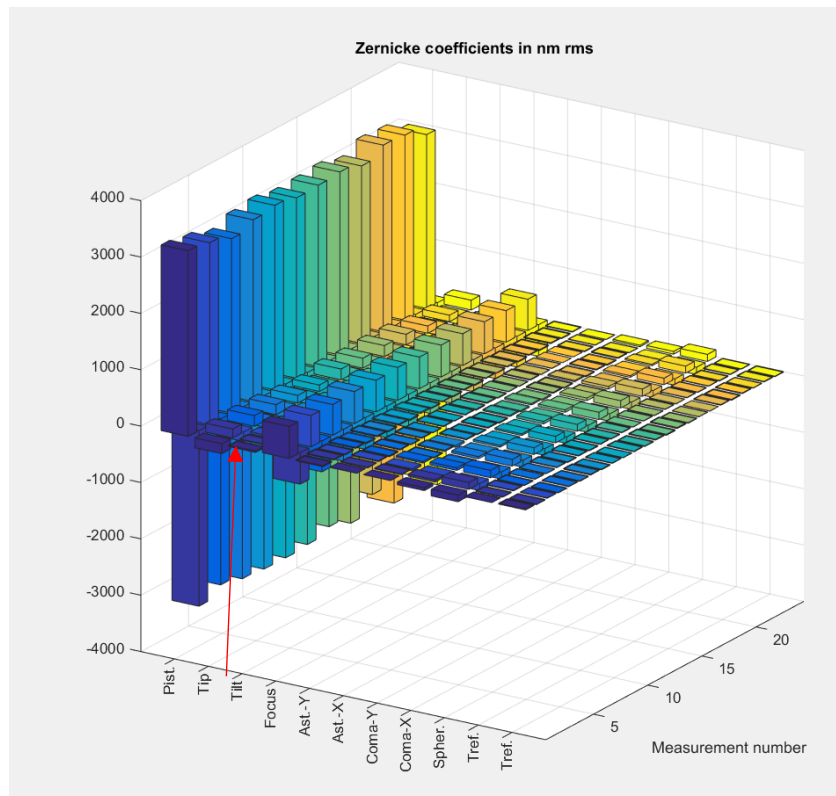


Figure 18. Modal purity of focus mode

Note that if the piston is not fitted, the focus tends to be overestimated and a large spherical mode appears as well (which in principle cannot be generated by the warping harness).

### Measurement of the influence functions and comparison with FEM

The derivation of the surface shape due to warping harness actuation has been computed in the Finite Element Modelling of the CESA support. Influence functions are defined as the deformation of the segment meshed surface at each node for each warping harness input, so 12 tables are available in total from which only 9 were used for this experiment. The actuation in the model for each function is 1 Nm at the proper degree of freedom.

A small discrepancy between the segment included in the model and the segment used for the experiment exists, which is a few millimetres difference in size, as the one for the model was a regular hexagon with average size, while the real one in the experiment was already shaped. This discrepancy is expected to cause negligible effects with respect to the distortion due to the warping harness.

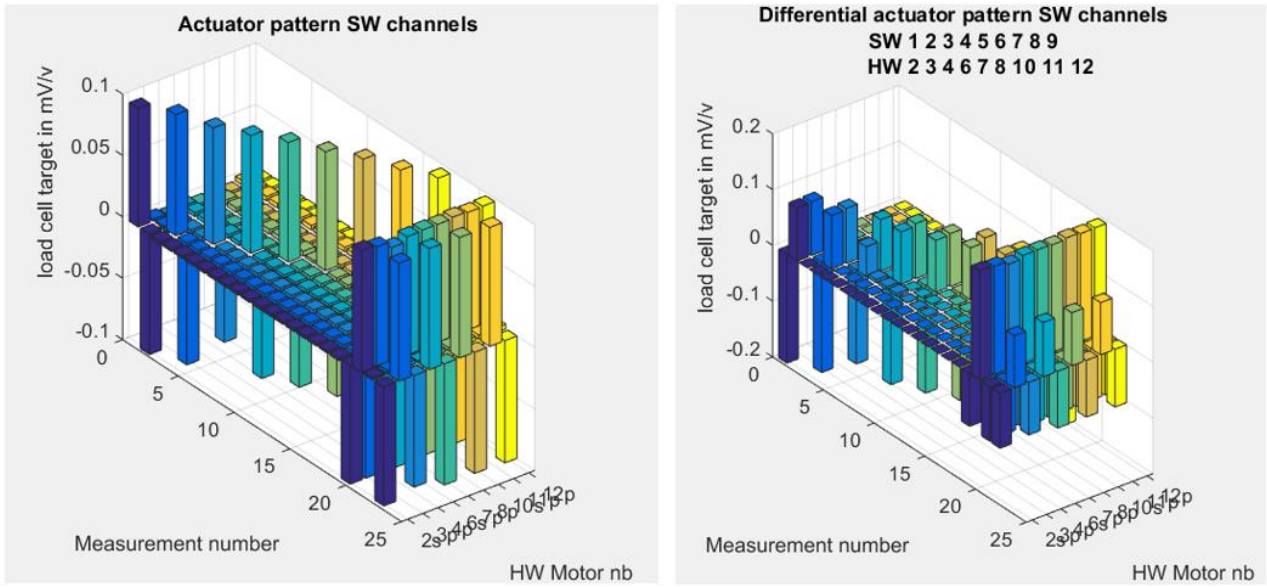


Figure 19. Test execution and load cell readings

We compared the results from the experiment with the FEM results, as shown in the following figures.

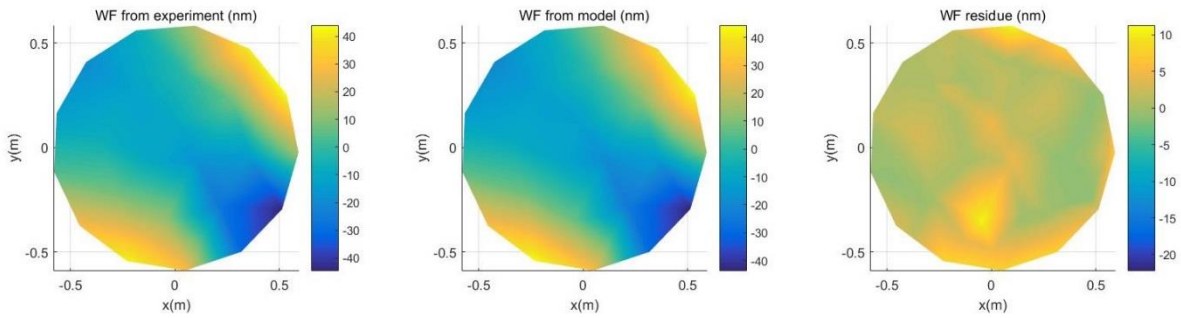


Figure 20. Influence function 1 (1 Nm)

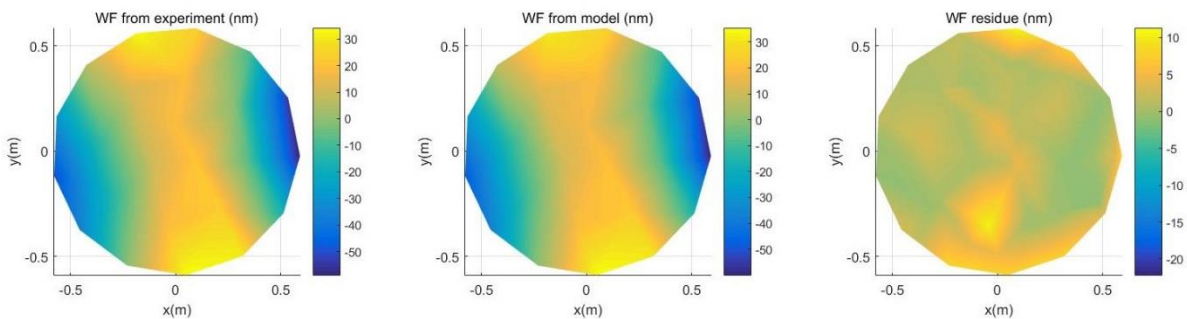


Figure 21. Influence function 2 (1 Nm)

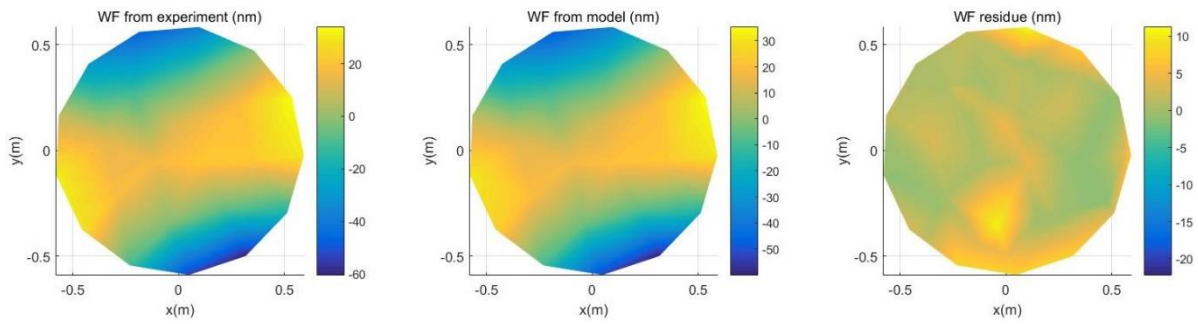


Figure 22. Influence function 3 (1 Nm)

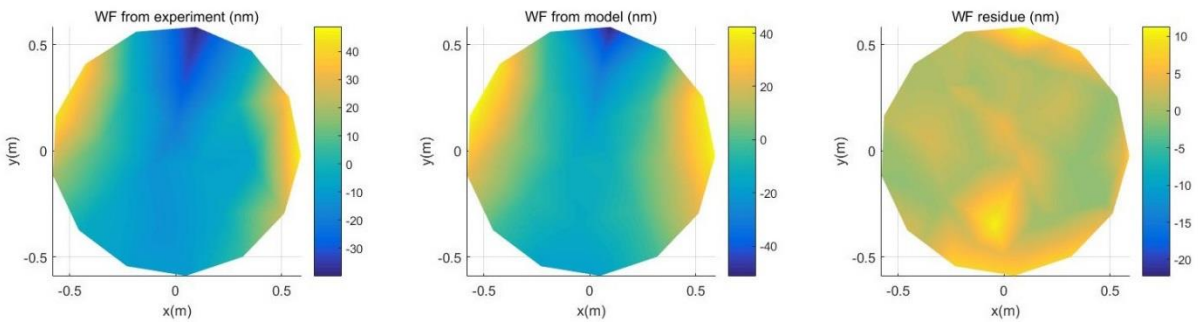


Figure 23. Influence function 4 (1 Nm)

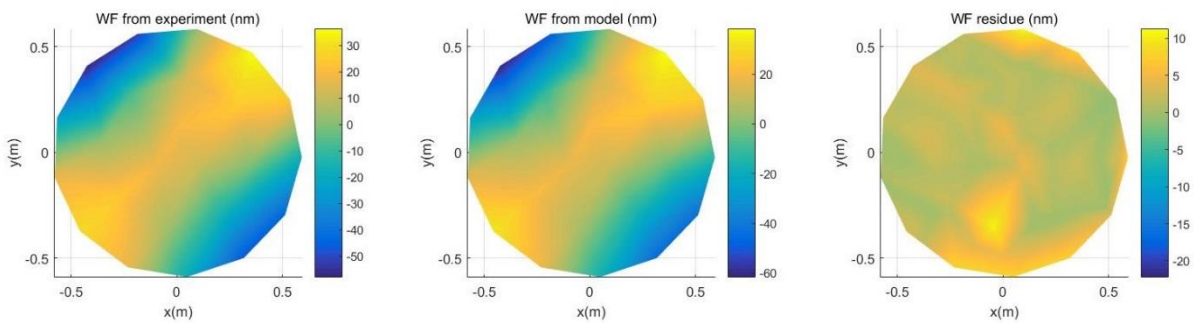


Figure 24. Influence function 5 (1 Nm)

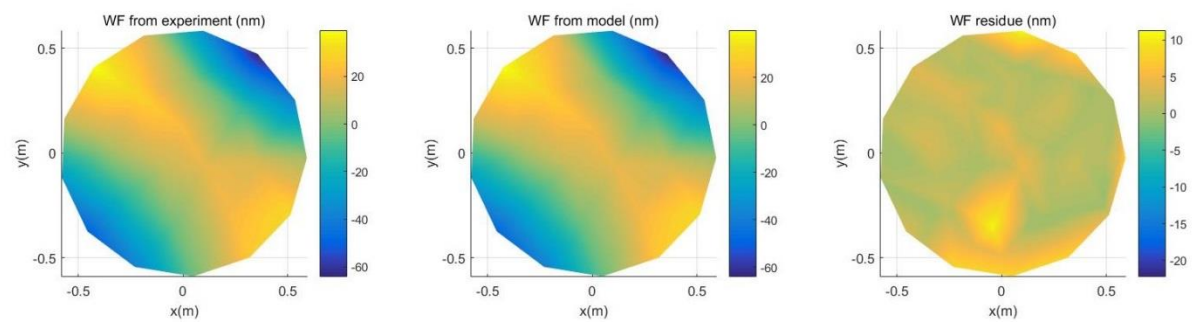


Figure 25. Influence function 6 (1 Nm)

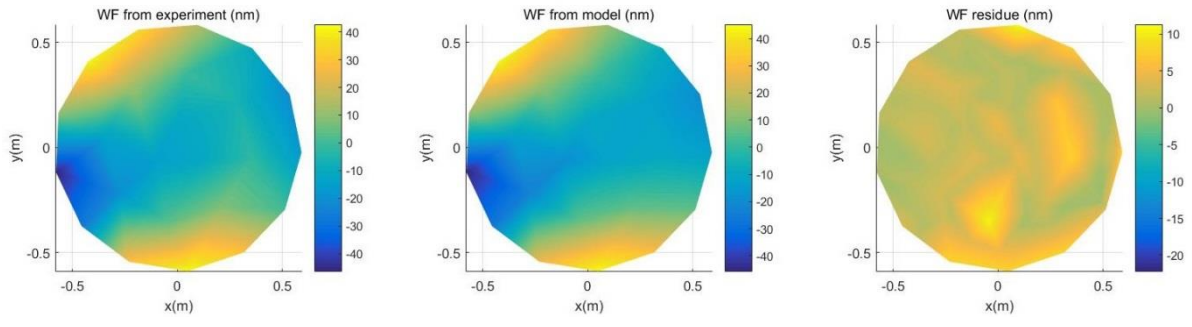


Figure 26. Influence function 7 (1 Nm)

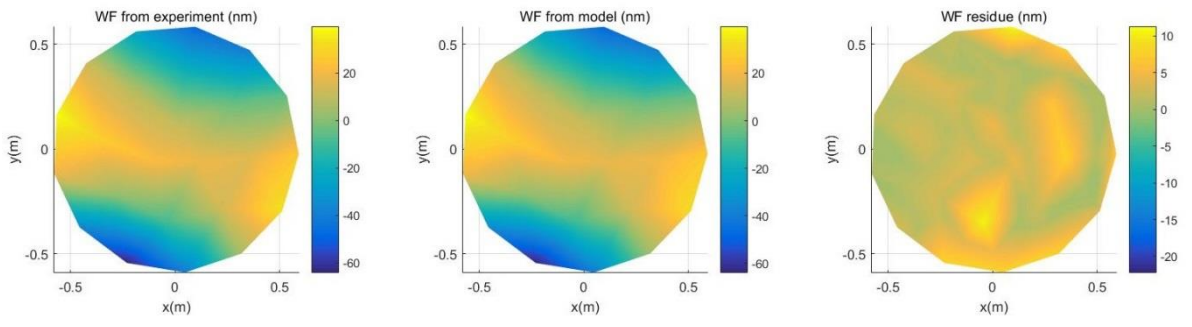


Figure 27. Influence function 8 (1 Nm)

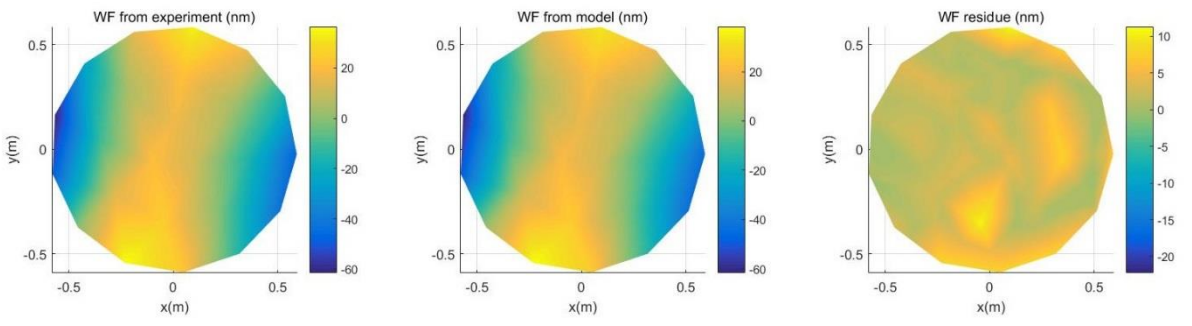


Figure 28. Influence function 9 (1 Nm)

Table 1 summarizes the results of the comparison. Residuals denote the absolute error: WF experiment – WF model. The relative error in percent is defined as  $100 \times (\text{rms residue} / \text{rms model})$ .

Table 1. Summary of influence functions comparison

Function	P2V test (nm)	P2V model (nm)	P2V residual (nm)	rms test (nm)	rms model (nm)	rms residual (nm)	Rel. error (%)
1	88.1	87.7	8.2	20.9	20.6	2.1	10.3
2	92.8	95.1	5.1	23.6	23.6	1.4	6.0
3	94.1	95.1	5.8	23.4	23.4	1.2	5.2
4	88.6	93.4	30.2	19.3	19.7	5.8	29.6
5	93.9	99.5	8.9	23.2	23.5	1.9	8.2
6	102.9	103.4	5.1	24.0	24.1	1.1	4.5
7	88.8	90.6	13.2	19.6	20.4	3.3	16.1
8	103.3	103.1	4.1	23.9	23.9	1.1	4.6
9	97.2	99.3	5.4	23.1	24.1	1.2	4.9

For comparison purposes between technologies, results from a similar measurement campaign performed at SAGEM under an interferometric tower on a CESA segment support are shown in Table 2 (no need to match the results on Table 1).

Table 2. Influence functions on interferometric tower measured by SAGEM

Function	rms test (nm)	rms model (nm)	rms residual (nm)	error (%)
1	48.7	207.9	21.8	10.5
2	78.3	206.3	20.5	9.9
3	320.0	247.1	21.5	8.7
4	285.6	249.4	25.3	10.1
5	88.8	205.9	25.9	12.6
6	78.7	206.0	20.5	10.0
7	290.7	249.6	30.7	12.3
8	332.4	245.9	25.8	10.5
9	74.8	207.1	32.8	15.8
10	69.5	204.5	24.2	11.8
11	297.3	248.0	15.0	6.0
12	284.4	249.6	13.8	5.5

## 5. Ramp Test

A further test consisted of applying the same torque to all 9 actuators and stepping through the torques with constant increments of 0.25 mV/V. Figure 27 shows the position increments as a function of actuation steps.

If the system of the actuators, whiffle tree, segment bending was perfectly linear and in the absence of measurement errors, one would expect constant measured position increments. However, there is a spike in the plot near  $-0.3$  mV/V, indicating that the position increments of the segment, coming from the left of the plot (i.e., negative mV/V values) grew to  $-1$   $\mu\text{m}$  near  $-0.5$  mV/V, then reduced, just to grow again and finally settle to values between  $-0.6$   $\mu\text{m}$  and  $-0.9$   $\mu\text{m}$ .

This letter-W-like motion looks like a stick-slip phenomenon. It has been conjectured that the nonlinearity of the response may have been caused by a buckling transition in the central segment membrane (“popping juice bottle lid”). The authors are planning to rerun this test on the qualification models. In any event, the experiment demonstrates the usefulness of a segment test stand that can measure piston, in addition to segment figure from bending.

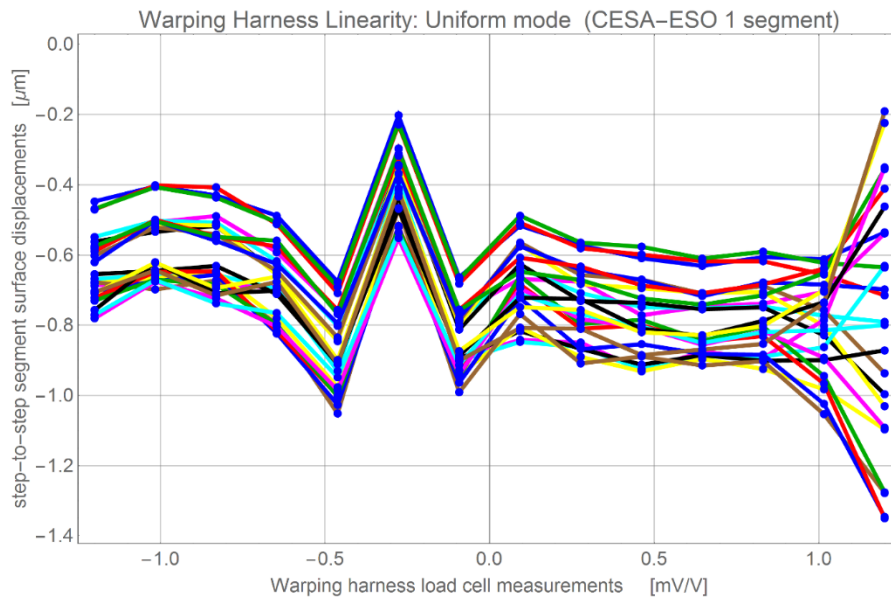


Figure 27. Ramp test with uniform actuation pattern

## 6. CONCLUSIONS AND PERSPECTIVES

- The “Absolute Multiline” metrology system by Etalon AG [2] coupled with the fiber plate configuration is considered capable of measuring the influence functions of the ELT segment warping harnesses [1] with adequate accuracy.
- This configuration represents a cost-effective and simple alternative to an interferometric setup for the detection of the modes that can be generated by the warping harness (i.e. by definition limited to “low” spatial modes). If necessary, such a system could easily be replicated at Armazones for the verification of the functionality of a segment support prior to re-integration in the telescope.
- With the current configuration, it would be possible to measure the segment deformation due to gravity provided that the segment is coated. The alternative would be to spend more design effort to improve the fiber collimator alignment sensitivity (the vendor indicated that a recent software update may fix this problem). A stiffer test setup is recommended to improve accuracy. Limitations were present due to recycling of already existing elements like the display cart.
- A similar test can be conducted in a relatively short time frame with the qualification models of the ELT segment support.
- The “Absolute Multiline” has now shown its high potential in a variety of telescope related applications, ranging from:
  - Mirror shape measurement (this work)
  - Detection of vibrations
  - Mirror rigid body motion monitoring
- The ELT instruments could also benefit from such a system, for example for the monitoring of structural deformation both for warm and cold optics (as demonstrated by CERN).

In summary, the Absolute Multiline system has proven to be a highly effective, accurate and extremely versatile measurement device. The cost/benefit ratio seems very favourable.

## 7. ACKNOWLEDGMENT

The authors would like to acknowledge Ralf Conzelmann for the design of the fiber plate, Martin Brinkmann for the finite-element analysis and Robert Frahm for control software support.

## REFERENCES

- [1] Rodolfo, J.; Chouarche, L. and Chaussat, G., *et al.*, "Prototype segments polishing and testing for ELT M1," Proc. SPIE **8450**, 845023 (2012); doi: 10.1117/12.925417
- [2] *Absolute Multiline* technology by Etalon AG, [online link](#)